Spectroscopic analysis of temperature and density of Sn plasma produced by a CO_2 laser

Nek M. Shaikh,[1,2,a] Y. Tao,[1] R. A. Burdt,[1] S. Yuspeh,[1] N. Amin,[1,3] and M. S. Tillack[1]
[1]*Center for Energy Research, University of California, San Diego, 9500 Gilman Drive, La Jolla, California 92093-0417, USA*
[2]*Institute of Physics, University of Sindh, Jamshoro 76080, Pakistan*
[3]*Department of Physics, University of Agriculture, Faisalabad 38040, Pakistan*

(Received 24 April 2010; accepted 3 July 2010; published online 22 October 2010)

The temporal and spatial evolution of electron temperature and electron density from Sn plasma produced by a CO_2 laser has been investigated in vacuum using spectroscopic methods. The plasma parameters were inferred by the Boltzmann plot method from experimentally observed line profiles of singly ionized Sn and Stark broadened profiles. At a laser intensity of 10^{10} W/cm^2, electron temperature and density were measured to be within 1.13 eV to 0.53 eV and 5.3×10^{16} cm^{-3} to 1.4×10^{16} cm^{-3}, respectively, for delay times between 200 ns and 1100 ns, and at distances up to 5 mm along the target normal. The results show the electron temperature and density from Sn plasma produced by a CO_2 laser with wavelength of 10.6 μm to be lower than previously reported results using a 1064 nm laser in a similar parameter regime. The lower temperature in the region far away from the target surface confirms the smaller interaction region for CO_2 laser as compared with that of neodymium-doped yttrium aluminum garnet laser. © *2010 American Institute of Physics*. [doi:10.1063/1.3475369]

I. INTRODUCTION

Laser-produced tin (Sn) plasma (LPP) is the most promising candidate for the next generation extreme ultraviolet (EUV) light source used in the semiconductor lithography industry to produce microchips with feature size of 22 nm or smaller.[1] Sn is considered as the source for EUV plasma due to its high conversion efficiency (CE) from laser to 13.5 nm (3% bandwidth) EUV emission.[2–5] In the development of EUV source, the in-band CE and debris (high-energy ions, atoms, and microdroplets) emitted from the plasma are the two most challenging issues. The debris limit the lifetime of the expensive and delicate Mo/Si multilayer collector. In this regard, most of the previous studies of Sn LPP have focused to increase the CE of the EUV light source and decrease the debris using different laser wavelength,[6–9] different pulse duration, and samples with different thickness and different percentage of Sn,[10] etc. Besides the measurement of the EUV light during the laser pulse, the researchers also studied the Sn ions and droplets at a longer distance from the target using Faraday cups and quartz crystal microbalance detectors.[11,12]

There have been minimal efforts to study the behavior of the Sn plasma after the end laser pulse produced by a 10.6 μm transversely excited atmosphere (TEA) CO_2. The objective of this study is to understand the expansion dynamics of the laser produced Sn plasma generated by the CO_2 laser. Electron temperature (T_e) and electron density (N_e) can be inferred using visible spectroscopy leading to additional insight into the behavior of the plume.

Previously, Harilal *et al.*[13] studied the space and time resolved plasma properties of the Sn LPP generated by a 1064 nm neodymium-doped yttrium aluminum garnet (Nd:YAG) laser with pulse duration of 8 ns. In the same paper, the authors estimated the T_e and N_e at a distance of 1 mm from the Sn surface were in the range of 3.2 eV and 7.7×10^{17} cm^{-3}, respectively. Torrisi and Margarone[14] studied the Sn plasma in a high vacuum (10^{-7} mbar) with different analysis techniques including ion collectors, mass quadrupole spectrometry, electron microscopy, and surface profilers. They investigated the high ablation yield and high fractional ionization of the low boiling point metallic elements, such as Sn, Al, and Pb, as a result of 1064 nm wavelength laser irradiation. O'Shay *et al.*[15] studied the hydrodynamic behavior of the Sn plume generated by 1064 nm laser irradiation. The maximum T_e and N_e were estimated as 1.4 eV and 4.1×10^{17} cm^{-3}, respectively, at a laser irradiance of 3.8×10^{11} W/cm^2. Alonso-Medina and Colo'n[16] also employed a laser-induced breakdown spectroscopy (LIBS) technique using 1064 nm Nd:YAG laser to measure the Stark widths of 43 spectral lines of Sn I and 27 spectral lines of Sn II. The electron number density and temperature were obtained from the Stark broadening profiles and Boltzmann plots, respectively, and found to be 0.95 eV and 1.1×10^{16} cm^{-3} at the laser intensity of 1.4×10^{10} W/cm^2.

Most recently, in our previous study, we investigated the effect of 1.064 μm Nd:YAG and 10.6 μm CO_2 lasers on the charge state resolved ion energy distribution of Sn plasma freely expanding in to the vacuum.[17] At the longer laser wavelength (10.6 μm), higher charge state ions were observed. In this study, we investigate the space and time evolution of electron temperature and electron density of the Sn plasma generated by 10.6 μm TEA CO_2 laser irradiation for the first time. We measure the temporal variation in the plume parameters at different positions along the target nor-

[a]Electronic mail: neksheikh@yahoo.com.

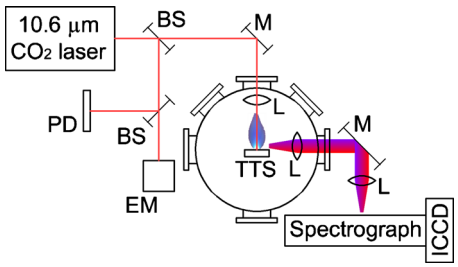

FIG. 1. (Color online) Experimental arrangement: BS—beam sampler, M—mirror, PD—photodiode, EM—laser energy monitor, TTS—target translation stage, L—lens, ICCD—intensified charge—coupled device camera, and spectrograph—Acton 500i SpectraPro.

mal direction of the plasma expansion. The effect of the self absorption and the minimum criteria for the local thermodynamic equilibrium (LTE) are also discussed.

II. EXPERIMENTAL SETUP

The experimental setup is shown in Fig. 1. Experiments were carried out using a short pulse master oscillator and power amplifier (MOPA) CO_2 laser system. The gas mixture ratio of the oscillator is (CO_2:N_2:He=20:4:76%), optimized to remove the long microsecond tail and enhance the peak power of the oscillator to 1 MW. The pulse duration of the laser from the oscillator is shortened by an air-breakdown plasma shutter. The plasma shutter is triggered by the free electrons from an air-breakdown plasma induced by a Q-switched Nd:YAG laser and pumped by the oscillator itself. Additional information about the MOPA laser can be found elsewhere.

A 2 mm thick pure Sn sample was mounted on a three-dimensional motorized stage inside a chamber evacuated to 10^{-5} torr. For the CO_2 laser, the pulse duration, focal spot size diameter, pulse energy, and resultant laser intensity are 84 ns, 200 μm, 130 mJ, and 10^{10} W/cm^2, respectively. The pulse duration and energy of the CO_2 laser varied by 15% over the course of the experiments due to degradation of the stationary gas in the laser cavity and variations in the ambient conditions of the laboratory. The CO_2 laser was focused onto the target surface at normal incidence by an F/10 meniscus lens placed inside a vacuum chamber. The target was translated in the focal plane before each shot to provide a fresh surface. The plume was observed in a plane orthogonal to the planar target surface with a 1:1 imaging system consisting of a collimating and focusing lens used to image the visible plasma radiation to the entrance slit of a 0.5 m Czerny–Turner spectrograph (Acton Pro, Spectra-Pro 500i). The spectrograph was equipped with three gratings: 150, 600, and 2400 groves/mm. The output of the spectrograph was coupled to an intensified charge-coupled device (ICCD) camera (PI MAX, Model 512 RB) that was operated with vertical binning of the 512×512 pixel array to provide spectral intensity versus wavelength. A programmable timing generator (Standford DG535) enables the acquisition of time resolved plasma spectra by controlling the delay between the laser pulse arrival and the detector system, as well as the intensification (exposure) time. The highest resolution of the 2400 groove/mm holographic grating were used for the better resolution to estimate the Stark broadening of the transition lines, these lines further used to estimate the N_e, whereas for the measurement of the T_e, 600 groove/mm grating was used.

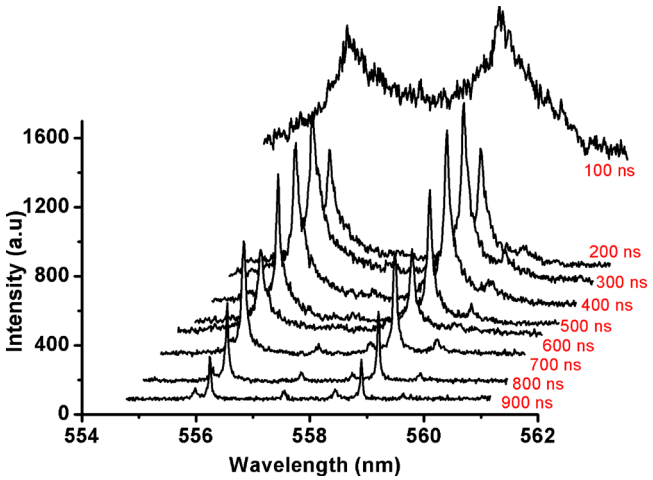

FIG. 2. (Color online) Temporal variation in the intensity and width of the Sn II (556.19 nm and 558.89 nm) transition line at different delay times.

III. RESULT AND DISCUSSION

The first set of experiments showed the temporal variation in the intensity and width of the transition lines of the Sn plume produce by the CO_2 laser having irradiance of 1.5 $\times 10^{10}$ W/cm^{-2}. The temporal variation in the intensity and width of the Sn (II) lines at 556.19 nm ($6d\ ^2D_{5/2} \rightarrow 6p\ ^2P_{3/2}$) and 558.89 nm ($4f\ ^2F_{5/2} \rightarrow 5d\ ^2D_{3/2}$) transition lines at different delay times is shown in Fig. 2. The identification of both lines is straight forward as all these transitions are listed in the National Bureau of Standards (National Institute of Standards and Technology) (NBS (NIST)) database.[18] The variation in the integrated intensity of Sn (II) lines at 556.19 and 558.89 nm at different delay times is shown in Fig. 3. At early stages of the plasma (0–200) ns a strong continuum is observed, which mainly results from the bremsstrahlung and electron ion recombination process. That intense continuum is converted into the well separated iso-

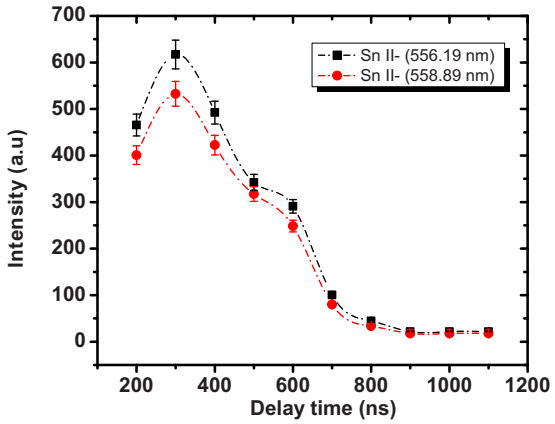

FIG. 3. (Color online) Temporal variation in the intensity of the 556.19 nm (black squares) and 558.89 nm (red circles) transition lines from Sn II at (200–1100) ns delay time.

lated lines at a delay of 200 ns. At a time 200 ns after the laser pulse, the line emission can be distinguished easily from the continuum. From (200–300) ns the emission intensity of the Sn (II) transition lines first increases, then decreases during the time duration (300–1100) ns due to the recombination.

A. Electron temperature (T_e)

The electron temperature has been determined using Boltzmann plot method in which the population of the excited states follows the Boltzmann distribution and their relative emissivity (I_{mn}) is given as[19–21]

$$\ln\left(\frac{\lambda_{mn}I_{mn}}{hcg_mA_{mn}}\right) = \ln\left(\frac{N(T)}{U(T)}\right) - \frac{E_m}{kT_e}, \quad (1)$$

where λ_{mn}, A_{mn}, and g_m are the wavelength, the transition probability, and the statistical weight of the upper level, respectively. E_m is the upper level energy, T_e is the electron temperature, k is the Boltzmann constant, $U(T)$ is the partition function, and $N(T)$ is the total number density of neutrals. From Eq. (1), a plot of $\ln(\lambda_{mn}I_{mn}/hcg_mA_{mn})$ versus E_m for the observed spectral lines is a straight line with a slope of $-1/kT_e$. Five Sn II lines at 533.23 nm ($6d\ ^2D_{3/2} \rightarrow 6p\ ^2P_{1/2}$), 556.19 nm ($6d\ ^2D_{5/2} \rightarrow 6p\ ^2P_{3/2}$), 558.89 nm ($4f\ ^2F_{5/2} \rightarrow 5d\ ^2D_{3/2}$), 645.35 nm ($6p\ ^2P_{3/2} \rightarrow 6s\ ^2S_{1/2}$), and 684.4 nm ($6p\ ^2P_{1/2} \rightarrow 6s\ ^2S_{1/2}$) have been employed in the Boltzmann plot method under the assumption of LTE.[22,24]

B. Electron density (N_e)

The shape and width of the spectral lines emitted by the plasma are governed by the collisional processes perturbing the emitting atoms and ions. Hence, the plasma density can be inferred from the profile of line spectra. The full width at half maximum of the Stark broadened profile of Sn (II) line at 556.19 nm has been used to estimate the electron number density.[22–24] The Stark broadening parameter ω was taken from Ref. 16. Spectroscopic constants of Sn (II) lines used for the estimation of temperature have been taken from the NIST database.[18]

The minimum criteria for LTE proposed by McWhirter[25] have also been verified using the relation

$$N_e \geq 1.6 \times 10^{12} T^{1/2} \Delta E^3, \quad (2)$$

where T (K) is the plasma temperature and ΔE (eV) is the energy difference between the states, which are expected to be in LTE. At Sn (II) line of 556.19 nm, $\Delta E = 2.325$ eV, $T = 13\ 000$ K, Eq. (2) yields the minimum electron number density $N_e \geq 2.2 \times 10^{15}$ cm^{-3} to justify the LTE assumption.

The use of emission spectroscopy for the measurement of temperature and electron number density requires optically thin spectral lines. The Sn plasma is observed to be optically thin when self absorption lines appear to have either a flat topped profile (saturation) or a dip at the central frequency (self absorption). The self absorption depends on the oscillator strength, level energies degeneracy, broadening parameters, and also on the plasma parameters.[26] In the present work, we did not find any saturation or dip at the central frequency of the observed emission lines.

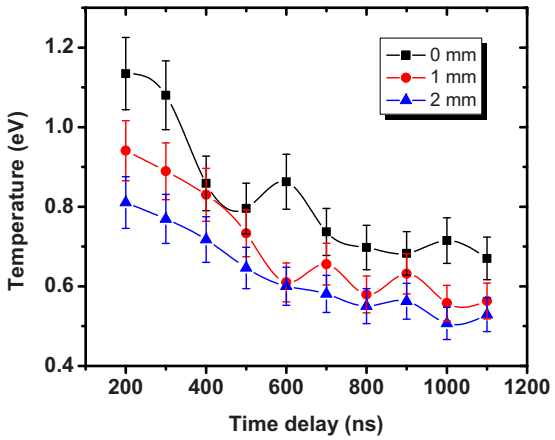

FIG. 4. (Color online) Temporal variation in the temperature of the Sn plume at 0 mm (black squares), 1 mm (red circles) and 2 mm (blue triangles) from the surface of the target at (200–1100) ns delay time.

In the first set of experiments, we have recorded the emission lines at different delay times to study the temporal evolution of the plasma parameters. The same experiment is repeated at three different positions of 0, 1, and 2 mm from the surface of the sample along the target normal to determine the spatial evolution of the plasma parameters. From the spectroscopic analysis of such transition lines, the T_e has been determined to be in the range (1.13–0.67) eV, (0.94–0.56) eV, and (0.81–0.53) eV, where as the N_e have been estimated as $(5.32 \times 10^{16} - 1.97 \times 10^{16})$ cm^{-3}, $(3.97 \times 10^{16} - 1.59 \times 10^{16})$ cm^{-3}, and $(2.3 \times 10^{16} - 1.47 \times 10^{16})$ cm^{-3} at the time delay of (200–1100) ns, respectively, shown in Figs. 4 and 5.

During irradiation of the target, the leading edge of the laser pulse rapidly heats and vaporizes material just above the surface, and the resultant plasma absorbs and reflects the remainder of the laser pulse. After the laser irradiation, the plasma expands adiabatically in three dimensions, and some thermalization may occur through electron ion collisions. The initial thermal energy is converted into kinetic energy of expansion through hydrodynamic phenomenon. Accordingly, the temperature and density of electrons will both be higher closer to the target surface, as observed in the experiments.

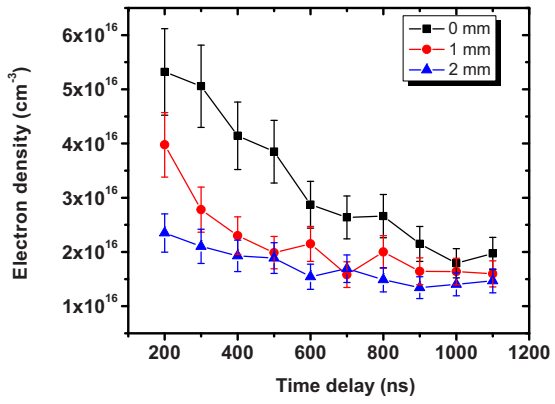

FIG. 5. (Color online) Temporal variation in the electron number density of the Sn plume at 0 mm (black squares), 1 mm (red circles) and 2 mm (blue triangles) from the surface of the plane Sn target at (200–1100) ns delay time.

The variation at the earlier stage of the plume is much higher than at later times because energy is regained in the recombination of the ions.

The decrease in the N_e is due to the three body recombination and radiative recombination process. The recombination rate coefficient for these processes is related to the probability of transition from a free electron state to a bound state, where the third body to conserve energy can be either a heavy particle or free electron. The recombination rate coefficient for three body process depends rather weakly on the ion type. The dependence of the recombination rate for the radiative and the three body recombination on the ion charge $\bar{Z}$, electron density N_e, ion density N_i and electron temperature T_e is $N_e N_i \bar{Z}^2 T^{-3/4}$ and $N_e^2 N_i \bar{Z}^3 T_e^{-9/2} \ln\sqrt{\bar{Z}^2+1}$, respectively.[27]

In the plasma the laser is primarily absorbed by inverse bremsstrahlung (IB) processes and direct single-photon processes (Zel'dovich and Raizer).[28] The IB absorption cross-sections for electron-neutral collisions are much lesser than that via electron ion collisions. The laser intensity absorbed by expanding plasma via the IB process from the incident laser beam at any time is given by[29,30]

$$I_{abs} = I_0(1 - e^{-\alpha_{IB}X}), \tag{3}$$

where α_{IB} is the average IB absorption coefficient of the plasma and X is the dimension of the plasma in the direction perpendicular to the laser beam. The α_{IB} via free electron is approximated from the expression[31–33]

$$\alpha_{IB}(\text{cm}^{-1}) = 1.37 \times 10^{-35} \lambda^3 N_e^2 T_e^{-1/2}. \tag{4}$$

Here $\lambda(\mu\text{m})$ is the wavelength of the laser photons, T_e (K) is the electron temperature, and N_e (cm^{-3}) is the electron density. The absorption and/or reflection of the laser photons by the plasma depend on the plasma frequency.

It has been well known that the optimum plasma density and temperature for efficient in-band 13.5 nm EUV emission are generally around $N_e \sim 10^{19}$ cm^{-3} and $T_e \sim 20-30$ eV, however their density profiles are very different with different laser wavelengths. For example, it has been shown that density profile of Sn plasma irradiated with CO_2 laser pulse is much steeper than that of Nd:YAG laser. The greater gradient in CO_2 laser produced Sn plasma produces a faster plasma expansion, resulting in a lower and cooler long-distance plasma as compared with that of Nd:YAG laser Sn plasma.

In the next set of experiments, we have studied the spatial variation in the plasma properties of the Sn LPP generated by the same experimental conditions as discussed earlier. In the case of the spatial variation in the plasma parameters T_e and N_e vary as (1.12–0.56) eV and ($5.45 \times 10^{16} - 5.9 \times 10^{15}$) cm^{-3} with the distance from (0–5) mm, respectively, shown in Fig. 6. It is much higher close to the surface, decreases rapidly at the initial stage due to the fast thermalization and recombination processes within the short distances, and exhibits relatively little variation at larger distances.

Previous work by O'Shay *et al.*[15] measured higher temperatures and electron densities using a 1.064 μm Nd:YAG laser than the work presented here The laser parameters in Ref. 15 are 1.064 μm wavelength, 58 μm spot size $\sim 3.8 \times 10^{11}$ W/cm^2 and 10 ns pulse lengths whereas we used a 10.6 μm, 200 μm, $\sim 1.5 \times 10^{10}$ W/cm^2, and 84 ns, respectively. The most important factor is the laser wavelength, which directly affects the critical electron density (N_{cr}). The critical electron density at which the plasma becomes opaque to laser radiation is inversely proportional to the incident laser wavelength: $N_{cr} = (1 \times 10^{21}/\lambda^2(\mu\text{m}))(\text{cm}^{-3})$. Thus critical electron density for 1.064 μm, Nd:YAG laser is two orders of magnitude greater than the CO_2 laser, whereas the optical depth of the 10.6 μm CO_2 laser in the target surface is less than the 1.064 μm Nd:YAG laser. This difference in laser absorption density explains the lower measured electron density in CO_2 laser-produce plasma plumes.

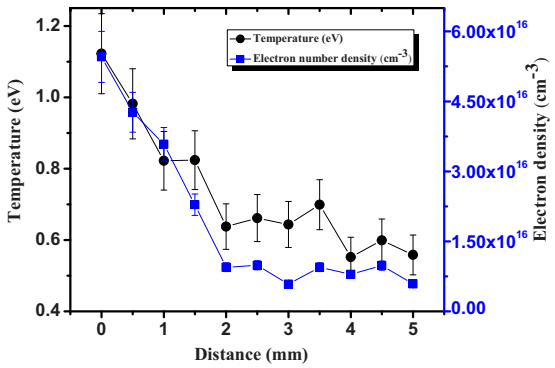

FIG. 6. (Color online) Spatial variation in the temperature (black circles) and electron number density (blue squares) of the Sn plume.

It can be assumed that the temperature in the core of the plasma for Nd:YAG and CO_2 is roughly the same (within a factor of 2) due to the fact that they both produce roughly the same EUV spectrum.[11] The lower absorption density in CO_2 produced plasma impacts the collision probability and recombination rate thus affecting the temperature of the plume after the laser pulse. The three body recombination rate depends upon the electron density, ion density as discussed earlier, so the recombination rate in the case of Nd:YAG LPP is much higher than the CO_2 laser, that give rise a lower density and a lower temperature. The lower temperature observed in CO_2 laser case as compared with that of Nd:YAG laser reveals a faster cooling down due to a faster plasma expansion, which may arise from the steeper gradient due to the smaller interaction region of CO_2 laser as compared with that of Nd:YAG laser, as pointed out in Ref. 34. The lower density is the combination effect of the lower critical density and the faster plasma expansion.

IV. CONCLUSION

A space and time-resolved diagnostic technique has been used to study the plasma properties of the Sn plume produced by the 10.6 μm CO_2 laser. The estimated value of the temperature and electron number density in the present work of the CO_2 laser are much lower than the reported work of the 1.064 μm Nd:YAG laser. One possible explanation of the lower temperature in the region far away from the target surface is the smaller interaction region in CO_2 laser with Sn

plasma as compared with that of Nd:YAG laser. The lower electron density is due to the combined effect of the lower critical density and smaller interaction region. It is inferred that lower value of the electron temperature and electron density in the case of CO_2 laser produced Sn plasma comes from the fact that CO_2 laser is more likely absorbed within a thinner layer near the target surface due to its long wavelength. This small penetration depth could lead to less ablation material with a CO_2 laser pulse as compared with that of a Nd:YAG laser.

ACKNOWLEDGMENTS

Dr. N. M. Shaikh and Dr. N. Amin are grateful to Higher Education Commission (HEC) of Pakistan for providing the scholarships for the post doctoral research work. Dr. N. M. Shaikh is also thankful to University of Sindh, Jamshoro, Pakistan for the grant of sabbatical leave.

[1]Y. Tao, M. S. Tillack, K. L. Sequoia, R. A. Burdt, S. Yuspeh, and F. Najmabadi, Appl. Phys. Lett. **92**, 251501 (2008).
[2]J. White, G. O'Sullivan, S. Zakharov, P. Choi, V. Zakharov, H. Nishimura, S. Fujioka, and K. Nishihara, Appl. Phys. Lett. **92**, 151501 (2008).
[3]Y. Ueno, G. Soumagne, A. Sumitani, A. Endo, and T. Higashiguchi, Appl. Phys. Lett. **91**, 231501 (2007).
[4]M. S. Tillack, K. L. Sequoia, and Y. Tao, J. Phys.: Conf. Ser. **112** 042060 (2008).
[5]Y. Tao, M. S. Tillack, S. S. Harilal, K. L. Sequoia, and F. Najmabadi, J. Appl. Phys. **101**, 023305 (2007).
[6]H. Tanaka, A. Matsumoto, K. Akinaga, A. Takahashi, and T. Okada, Appl. Phys. Lett. **87**, 041503 (2005).
[7]A. Takahashi, D. Nakamura, K. Tamaru, T. Akiyama, and T. Okada, J. Phys.: Conf. Ser. **112**, 042059 (2008).
[8]J. White, P. Dunne, P. Hayden, F. O'Reilly, and G. O'Sullivan, Appl. Phys. Lett. **90**, 181502 (2007).
[9]K. Okazaki, D. Nakamura, T. Akiyamaa, K. Toya, A. Takahashi, and T. Okada, Proc. SPIE, **7201** 72010T (2009).
[10]S. Fujioka, H. Nishimura, K. Nishihara, Akira Sasaki, A. Sunahara, T. Okuno, N. Ueda, T. Ando, Y. Tao, Y. Shimada, K. Hashimoto, M. Yamaura, K. Shigemori, M. Nakai, K. Nagai, T. Norimatsu, T. Nishikawa, N. Miyanaga, Y. Izawa, and K. Mima, Phys. Rev. Lett. **95**, 235004 (2005).
[11]A. Takahashi, D. Nakamura, K. Tamaru, T. Akiyama, and T. Okada, Appl. Phys. B: Lasers Opt. **92**, 73 (2008).
[12]R. A. Burdt, S. Yuspeh, K. L. Sequoia, Y. Tao, M. S. Tillack, and F. Najmabadi, J. Appl. Phys. **106**, 033310 (2009).
[13]S. S. Harilal, B. O'Shay, M. S. Tillack, and M. V. Mathew, J. Appl. Phys. **98**, 013306 (2005).
[14]L. Torrisi and D. Margarone, Plasma Sources Sci. Technol. **15**, 635 (2006).
[15]B. O'Shay, F. Najmabadi, S. S. Harilal, and M. S. Tillack, J. Phys.: Conf. Ser. **59**, 773 (2007).
[16]A. Alonso-Medina and C. Colo'n, Astrophys. J. **672**, 1286 (2008).
[17]R. A. Burdt, Y. Tao, M. S. Tillack, S. Yuspeh, N. M. Shaikh, E. Flaxer, and F. Najmabadi, J. Appl. Phys. **107**, 043303 (2010).
[18]Handbook of Basic Atomic Spectroscopic Data, NIST, http://physics.nist.gov/PhysRefData/Handbook/Tables/tintable4.htm
[19]J. S. Cowpe, J. S. Astin, R. D. Pilkington, and A. E. Hill, Spectrochim. Acta, Part B **63**, 1066 (2008).
[20]S. Hafeez, N. M. Shaikh, and M. A. Baig, Laser Part. Beams **26**, 41 (2008).
[21]S. Hafeez, N. M. Shaikh, B. Rashid, and M. A. Baig, J. Appl. Phys. **103**, 083117 (2008).
[22]H. R. Griem, Phys. Rev. **131**, 1170 (1963).
[23]T. Fujimoto and R. W. P. McWhirter, Phys. Rev. A **42**, 6588 (1990).
[24]A. Lesage, New Astron. Rev. **52**, 471 (2009).
[25]R. W. P. McWhirter, in *Plasma Diagnostic Techniques*, edited by R. H. Huddlestone and S. L. Leonard (Academic, New York, 1965), Chap. 5.
[26]B. Le Drogoff, J. Margot, M. Chaker, M. Sabsabi, O. Barthélemy, T. W. Johnston, S. Laville, F. Vidal, and Y. von Kaenel, Spectrochim. Acta, Part B **56**, 987 (2001).
[27]Abhilasha, P. S. R.Prasad, and R. K. Thareja, Phys. Rev. E **48**, 2929 (1993).
[28]Ya. R. Zel'dovich and Yu. P. Raizer, *Physics of Shock Waves and High-Temperature Hydrodynamic Phenomena* (Dover, Cambridge, Massachusetts, 2001).
[29]J. L. Miller and E. Friedman, *Photonics Rules of Thumb* (McGraw-Hill, New York, 2003).
[30]E. G. Gamaly, A. V. Rode, and B. Luther-Davies, J. Appl. Phys. **85**, 4213 (1999).
[31]R. K. Singh, O. W. Holland, and J. Narayan, J. Appl. Phys. **68**, 233 (1990).
[32]S. S. Harilal, C. V. Bindhu, R. C. Issac, V. P. N. Nampoori, and C. P. G. Vallabhan, J. Appl. Phys. **82**, 2140 (1997).
[33]J. J. Chang and B. E. Warner, Appl. Phys. Lett. **69**, 473 (1996).
[34]Y. Tao, Y. Ueno, S. Yuspeh, R. A. Burdt, N. Amin, N. M. Shaikh, M. S. Tillack, and F. Najmabadi, Proc. SPIE **7636**, 76360D (2010).